Impact parameter dependence of the disappearance of flow and in-medium nucleon-nucleon cross section

Suneel Kumar, Manoj K. Sharma, and Rajeev K. Puri
Department of Physics, Panjab University, Chandigarh -160 014, India

Karn P. Singh and I. M. Govil
Department of Physics, Cyclotron Laboratory, Panjab University, Chandigarh -160 014, India
(Received 4 May 1998)

The impact parameter dependence of the disappearance of nuclear flow is examined within the framework of the quantum molecular dynamics model. We confront the model with recent experimental findings of He *et al.* who measured the balance energy at different impact parameters for the reaction $^{64}Zn+^{27}Al$. We simulate the heavy ion collisions with different nucleon-nucleon cross sections which includes the energy-dependent cross section, in-medium cross section (G matrix), and several constant and isotropic cross sections. Our calculations show that the balance energy in central collisions can be explained nicely with standard energy-dependent cross section whereas one needs a larger cross section to explain the balance energy at peripheral collisions. [S0556-2813(98)06009-9]

PACS number(s): 24.10.Lx, 13.75.Cs, 25.70.Pq

I. INTRODUCTION

The nuclear reaction dynamics at incident energies between 10 MeV/nucleon and 1 GeV/nucleon yields several interesting phenomena such as the incomplete fusion, multifragmentation, nuclear flow, subthreshold particle production, etc. The reaction dynamics at low incident energies is governed by the attractive mean field whereas the repulsive interaction decides the fate of a reaction at higher incident energies. At low energies, the Pauli principle hinders the nucleon-nucleon collisions and thus, the nucleon-nucleon collisions are nearly absent. In contrast, the effect of the Pauli principle at higher incident energies is very small and thus, the probability of nucleon-nucleon collisions increases.

Very recently, it was observed (in experiments) and predicted (in theories) that the interactions at higher incident energies are dominated by the nucleon-nucleon scattering which causes the particle emission in forward center of mass angles and hence the nuclear flow is positive. On the contrary, the interaction at low incident energies is dominated by the attractive part of the nuclear mean field which results in the particle emission at backward angles and hence the collective flow is negative. While going from low to high bombarding energies, the attractive and the repulsive parts of the interaction balance each other at some bombarding energy and hence the flow disappears. This particular energy at which the flow disappears is termed as the balance energy [1–15]. In recent years, several efforts have been made to pin down this balance energy accurately. Several different types of experimental attempts are made. The first category of experiments deals with the central collisions and one determines the balance energy for collisions involving a variety of colliding partners [3,4,14]. The colliding partners can be as light as carbon or as heavy as La. The balance energy in central collisions is found to vary as $A_{\rm tot}^{-1/3}$ (where $A_{\rm tot}$ is the total mass of target + projectile) [14]. The (measured) balance energy for the central collision of C + C is 127 ± 5 MeV/nucleon whereas it is about 50 MeV/nucleon for La + La [3,4,14]. Apart from the mass dependence of the disappearance of flow, another factor which affects the balance energy is the impact parameter [1,2,6–8,12,15]. Due to less compression in peripheral collisions, a large value of incident energy is needed to compensate the attractive mean field and hence the flow disappears at larger incident energy compared to central collisions. Recently, several systematic experiments have been carried out where impact parameter dependence of the disappearance of flow is investigated [1,8,12]. He *et al.* did the experiment of $^{64}Zn+^{27}Al$ [1] whereas Pak *et al.* performed $^{40}Ar+^{45}Sc$ [8,12]. The unique outcome of these experiments is that the balance energy increases linearly with change in the impact parameter.

Theoretically, one has a one body model such as the Boltzmann-Uhlening-Uhlenbeck (BUU) model [1,3–5,11,14], or a many body model such as the quantum molecular dynamics (QMD) model [7,10,15–17]. Both models are shown to work well in explaining the disappearance of flow. The main interest in measuring the disappearance of flow or predicting the same is that the balance energy is found to be very sensitive towards different nucleon-nucleon cross sections whereas it is relatively less sensitive towards different equations of state. In other words, by studying the balance energy, one can extract the information about the magnitude of the nucleon-nucleon cross section. In a couple of theoretical studies, a strong dependence of momentum force on disappearance of flow has been reported [7]. Here we confront the quantum molecular dynamics (QMD) model with the experimental observation of He *et al.* [1] who measured the balance energies as a function of impact parameter in the collision of $^{64}Zn+^{27}Al$. Our aim is to study the role of different nucleon-nucleon cross sections in determining the balance energy as a function of the impact parameter. We shall show here that one needs a larger cross section to explain the (experimentally) observed balance energy in peripheral collisions. In other words, one needs an additional repulsion which can be supplied either by assum-

ing a larger cross section or by taking momentum dependence of the mean field.

A similar study using the BUU model was also reported by He *et al.* [1]. They simulated the $^{64}Zn+^{27}Al$ reaction (using the BUU model) by varying the cross section between 25 and 55 mb. They found that a smaller cross section explains the data in central collisions whereas a larger cross section is needed to explain the data at semicentral/peripheral collisions. Here we employ a variety of cross sections instead, which includes the standard energy-dependent, isotropic and energy-independent and in-medium cross sections. In the following, we first describe briefly the QMD model and different nucleon-nucleon cross sections and then explain our results.

II. QUANTUM MOLECULAR DYNAMICS MODEL

We describe the time evolution of a heavy ion reaction within the quantum molecular dynamics model [16] which is based on the molecular dynamics picture. Here each nucleon is represented by the Wigner density of a Gaussian wave packet with a fixed width. In the QMD, each nucleon is represented by a coherent state of the form

$$\phi_\alpha(x_1,t)=\left(\frac{2}{L\pi}\right)^{3/4} e^{-[x_1-x_\alpha(t)]^2} e^{ip_\alpha(x_1-x_\alpha)} e^{-ip_\alpha^2 t/2m}. \tag{1}$$

Thus, the wave function has two time-dependent parameters x_α and p_α. The total n-body wave function is assumed to be a direct product of coherent states:

$$\phi=\phi_\alpha(x_1,x_\alpha,p_\alpha,t)\phi_\beta(x_2,x_\beta,p_\beta,t)\cdots, \tag{2}$$

where antisymmetrization is neglected. The initial values of the parameters are chosen in a way that the ensemble (A_T+A_P) nucleons give a proper density distribution as well as a proper momentum distribution of the projectile and target nuclei. The time evolution of the system is calculated by means of a generalized variational principle. We start out with the action

$$S=\int_{t_1}^{t_2}\mathcal{L}[\phi,\phi^*]d\tau, \tag{3}$$

with the Lagrange functional

$$\mathcal{L}=\left\langle \phi\left| i\hbar\frac{d}{dt}-H\right|\phi\right\rangle, \tag{4}$$

where the total time derivative includes the derivatives with respect to the parameters. The time evolution is obtained by the requirement that the action is stationary under the allowed variation of the wave function

$$\delta S=\delta\int_{t_1}^{t_2}\mathcal{L}[\phi,\phi^*]dt=0. \tag{5}$$

If the true solution of the Schrödinger equation is contained in the restricted set of wave function $\phi_\alpha(x_1,x_\alpha,p_\alpha)$, this variation of the action gives the exact solution of the Schrödinger equation. If the parameter space is too restricted, we obtain that wave function in the restricted parameter space which comes close to the solution of the Schrödinger equation. Performing the variation with the test wave function (2), we obtain for each parameter λ the Euler-Lagrange equation

$$\frac{d}{dt}\frac{\partial\mathcal{L}}{\partial\dot{\lambda}}-\frac{\partial\mathcal{L}}{\partial\lambda}=0. \tag{6}$$

For each coherent state and a Hamiltonian of the form $H=\Sigma_i[T_i+\frac{1}{2}\Sigma_{ij}V_{ij}]$, the Lagrangian and the Euler-Lagrange function can be easily calculated [16]:

$$\mathcal{L}=\sum_\alpha \dot{x}_\alpha p_\alpha-\sum_\beta\langle V_{\alpha\beta}\rangle-\frac{3}{2Lm}, \tag{7}$$

$$\dot{\vec{x}}_\alpha=\frac{p_\alpha}{m}+\nabla_{p_\alpha}\sum_\beta\langle V_{\alpha\beta}\rangle, \tag{8}$$

$$\dot{\vec{p}}_\alpha=-\nabla_{\vec{x}_\alpha}\sum_\beta\langle V_{\alpha\beta}\rangle. \tag{9}$$

Thus, the variational approach has reduced the n-body Schröndinger equation to a set of $6n$ different equations for the parameters which can be solved numerically. If one inspects the formalism carefully, one finds that the interaction potential which is actually the Bruckner G matrix can be divided into two parts: (i) a real part and (ii) an imaginary part. The real part of the potential acts like a potential whereas the imaginary part is proportional to the cross section. Here we discuss each of these inputs briefly.

A. The interaction potential [16]

The nucleons in QMD interact via a Skyrme potential and by Coulomb interaction. One has also an option of supplying an additional momentum-dependent interaction. As we plan to discuss the role of different nucleon-nucleon cross sections, we restrict ourselves to a simple static interaction supplemented by the Coulomb interaction

$$V_{ij}=V_{\rm loc}^2+V_{\rm loc}^3+V_{\rm Coul}. \tag{10}$$

The expectation value of these potentials is calculated as

$$V_{\rm loc}^2=\int f_i(\vec{p}_i,\vec{r}_i,t)f_j(\vec{p}_j,\vec{r}_j,t)V_I^{(2)}(\vec{r}_i,\vec{r}_j)\times d^3\vec{r}_i d^3\vec{r}_j d^3\vec{p}_i d^3\vec{p}_j, \tag{11}$$

$$V_{\rm loc}^3=\int f_i(\vec{p}_i,\vec{r}_i,t)f_j(\vec{p}_j,\vec{r}_j,t)f_k(\vec{p}_k,\vec{r}_k,t)V_I^{(3)}(\vec{r}_i,\vec{r}_j,\vec{r}_k)\times d^3\vec{r}_i d^3\vec{r}_j d^3\vec{r}_k d^3\vec{p}_i d^3\vec{p}_j d^3\vec{p}_k, \tag{12}$$

where $f_i(\vec{p}_i,\vec{r}_i,t)$ is the Wigner density which corresponds to the wave functions [Eq. (2)]. If we deal with local Skyrme force only, we get

$$V^{\rm Skyrme}=\sum_{i=1}^{A_T+A_P}\left[\frac{\alpha}{2}\left(\sum_{j=1}\frac{\tilde{\rho}_{ij}}{\rho_0}\right)+\frac{\beta}{\gamma+1}\sum_{j\neq i}\left(\frac{\tilde{\rho}_{ij}}{\rho_0}\right)^\gamma\right]. \tag{13}$$

Here α, β, and γ are the Skyrme parameters which are defined according to the ground state properties of a nucleus. In the present study, we use a hard equation of state with $\alpha = -124$ MeV, $\beta = 70.5$ MeV, and $\gamma = 2$. The interaction density $\tilde{\rho}_{ij}$ reads

$$\tilde{\rho}_{ij} = \frac{1}{(4\pi L)^{3/2}} e^{-\vec{r}_{ij}^{\,2}/4L}, \tag{14}$$

where $\vec{r}_{ij}$ is the distance between centroids of two Gaussians. In the present study, we also include the Yukawa interaction. Note that the symmetry potential is neglected in the present mean field. In addition, we have an average Coulomb force in the simulations. These effects influences the reaction dynamics at low energy whereas their effect at higher incident energies is small.

B. The nucleon-nucleon (NN) cross sections

The carefully initialized nuclei are displayed by a certain distance in coordinate space and boosted towards each other on Coulomb trajectories. During the propagation, two nucleons are supposed to suffer a collision if the distance between their centroids $|x_\alpha - x_\beta|$ is less than $\sqrt{\sigma/\pi}$. One also checks the availability of the final phase space with the so-called *classical Pauli procedure*. In this procedure, a collision is blocked if the phase space of the final state particles is already occupied. We here assume different forms of nucleon-nucleon cross sections $[\sigma]$ to understand their influence on disappearance of flow or on the balance energy. In the following, we describe the different nucleon-nucleon cross sections which will be used for analysis.

1. Energy-dependent cross section [19]

This energy-dependent cross section is a fit to the experimental cross section. This cross section is labeled as ''Cug.'' In this parametrization, the elastic and in-elastic cross sections are calculated as

$$\sigma_{nn}^{(e)}(\text{mb}) = \begin{cases} 55 & \text{if } \sqrt{s} < 1.8993, \\ \dfrac{35}{1 + 100(\sqrt{s} - 1.8993)} + 20 & \text{if } \sqrt{s} \geqslant 1.8993, \end{cases} \tag{15}$$

and

$$\sigma_{nn\to n\Delta}^{(in)}(\text{mb}) = \begin{cases} 0 & \text{if } \sqrt{s} < 2.015, \\ \dfrac{20(\sqrt{s} - 2.015)^2}{0.015 + (\sqrt{s} - 2.015)^2} & \text{if } \sqrt{s} \geqslant 2.015. \end{cases} \tag{16}$$

Here $\sqrt{s}$ is the nucleon-nucleon center-of-mass energy. For the elastic channel, the angular distribution $[d\sigma/dt] = ae^{bt}$ with $t = -2p^2(1 - \cos\theta)$. In case of inelastic channel, we use an isotropic distribution. We shall also use a modified version of the energy-dependent cross section where we have the same energy dependence but with an isotropic distribution. This comparison will give us a possibility to examine the role of angular distribution on flow.

2. Realistic G-matrix cross section [20]

The scattering of nucleons in nuclear matter in low-density expansion should be described in terms of the Bruckner G matrix

$$G(E) = V + V\frac{Q}{E - e + iE} G(E), \tag{17}$$

where the Pauli operator Q projects on unoccupied states and e is the energy of the intermediate state, $e = \vec{p}_1^{\,2}/2m + \vec{p}_2^{\,2}/2m + U(\vec{p}_1) + U(\vec{p}_2)$, where $\vec{p}_1$, $\vec{p}_2$ are the momenta of two colliding nucleons. At higher energies, the influence of the Pauli principle is small and the kinetic energy is large compared to the Hartree-Fock potential U. In this case, the G matrix becomes identical to the transition matrix which describes the scattering between two free nucleons. The cross section, thus derived, depends not only on the energy but also on density of the surrounding nucleons (and hence on the medium). It gives us information about the in-medium dependence of the nucleon-nucleon cross section. The G-matrix cross section is labeled as ''GMC.''

3. A constant cross section

At low energies, there are several calculations which are based on constant cross sections. Here, we also use isotropic and energy independent cross sections with $\sigma = 55$, 40, and 20 mb, respectively.

III. RESULTS AND DISCUSSION

We here simulate the ^{64}Zn+^{27}Al for 500–2000 events at different impact parameters using the abovementioned five nucleon-nucleon cross sections. We employ (i) an in-medium cross section based on Bruckner G matrix, (ii) an energy-dependent nucleon-nucleon cross section fitted by Cugnon, and (iii) three constant and isotropic cross sections with magnitude $\sigma = 55$, 40, and 20 mb, respectively. A hard equation of state is used in present analysis. Several recent studies show that the effect of different equations of state on balance energy is small [1,2,14]. In the present study, we neglect the momentum dependence of the force which is shown to have a strong effect on disappearance of flow at peripheral collisions [7,10,12].

There are several methods of defining the nuclear (sidewards) flow. Usually, the balance energy is extracted from $\langle p_x/A \rangle$ plots, i.e., the in-plane transverse momentum as a function of the normalized rapidity ($y_{\text{c.m.}}/y_{\text{beam}}$). By a linear fit to the slope of these curves, one can define the so-called reduced flow (F). By plotting F as a function of the beam energy, one obtains the balance energy E_{bal} as a point where a linear fit of the energy dependence of F passes through zero. This $\langle p_x/A \rangle$ plot is similar to a function of the rapidity bins. One can have a rather more integrated quantity called the ''directed transverse momentum'' $\langle p_x^{\text{dir}} \rangle$ which is defined as [10,16]

$$\langle p_x^{\text{dir}} \rangle = \frac{1}{N} \sum_i^N \text{sgn}[y_{\text{c.m.}}^{(i)}] p_x^{(i)}, \tag{18}$$

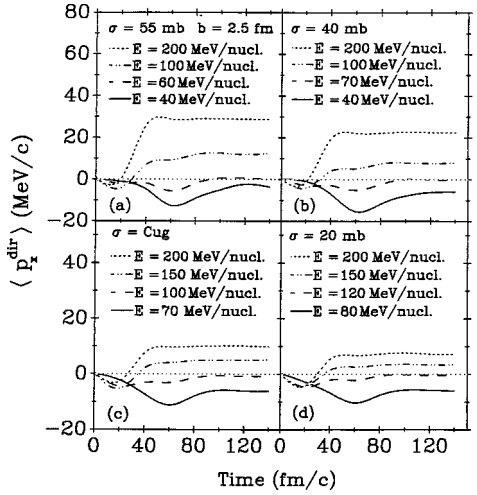

FIG. 1. The time evolution of averaged $\langle p_x^{\rm dir}\rangle$ as a function of time. Here we simulate ^{64}Zn+^{27}Al for 500–2000 events at each bombarding energy. (a), (b), (c), and (d) are the simulations using $\sigma=55$, 40 mb, Cugnon, and 20 mb, respectively. Note that different lines in different parts of the figure represent different incident energies.

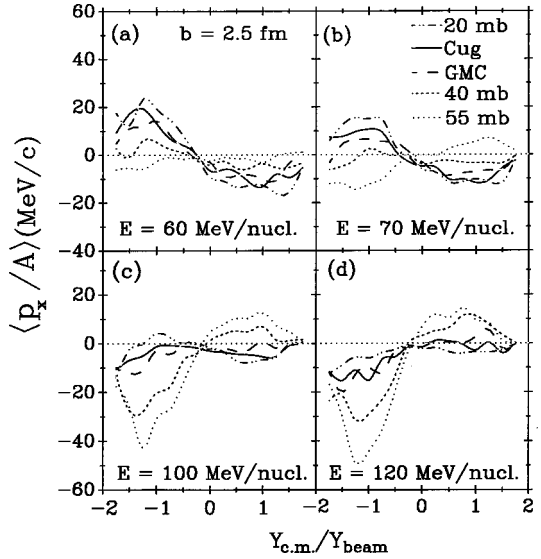

FIG. 2. Averaged $\langle p_x/A\rangle$ as a function of $Y_{\rm c.m.}/Y_{\rm beam}$. Here each part of the figure is a result at fixed incident energies. The various curves in each part of the figure indicate the results with different nucleon-nucleon cross sections. The solid line is for Cugnon, long dashed line for GMC, dotted for 55 mb, short dashed line for 40 mb, and dash-dotted for 20 mb. (a), (b), (c), and (d) are at incident energies of 60, 70, 100, and 120 MeV/nucleon, respectively.

with $p_x^{(i)}$ being the transverse momentum of the ith particle and where $y_{\rm c.m.}^{(i)}$ is the associated rapidity of the ith particle. In transverse momentum, all rapidity bins are taken into account. Therefore, this provides one value as a measure of the in-plane flow instead of a complicated function such as the $\langle p_x/A\rangle$ plot. In several experiments, it was shown that the balance energy $E_{\rm bal}$ is nearly independent of the nature of the particle. The balance energy is nearly the same for nucleons, light, and heavy fragments. Note that the fragments have larger flow compared to nucleons. Furthermore, the balance energy is insensitive to the apparatus corrections and acceptance and hence makes it possible to compare the unfiltered results of the theory with experimental findings.

It has been shown in Refs. [10,16] that $\langle p_x^{\rm dir}\rangle$ and $\langle p_x/A\rangle$ are equivalent. We here discuss both these quantities for the sake of completeness. In Fig. 1, we show the time evolution of $\langle p_x^{\rm dir}\rangle$ at different bombarding energies using nucleon-nucleon cross sections taken from Cugnon, a constant cross section $\sigma=55$, 40, and 20 mb, respectively. Note that the different curves in each part of the figure are at different incident energies. The (a), (b), (c), and (d) parts of the Fig. 1 are, respectively, with cross sections of 55, 40 mb, Cugnon, and 20 mb. We see that the flow first becomes negative and finally it saturates either at $-ve$ or $+ve$ values depending on the bombarding energy. The negative flow at the start of reaction signifies the attractive nuclear interactions at the start. At low incident energies, due to the lack of available phase space, we have few nucleon-nucleon collisions and as a result, the nuclear interactions are still attractive. At higher incident energies, however, one has frequent nucleon-nucleon collisions and therefore, nuclear flow is repulsive at the end of the simulations. One also notices that a larger cross section can have more (allowed) collisions and thus, the flow becomes positive at lower incident energies compared to that of smaller cross section. The flow $\langle p_x^{\rm dir}\rangle$ becomes zero at 60, 70, 100, and 120 MeV/nucleon for simulations with $\sigma=55$, 40 mb, Cug/GMC, and 20 mb, respectively. One also notices that it takes more time at low incident energies before the flow saturates. For example, the simulations with 55 mb at 40 MeV/nucleon take about 120 fm/c before they saturate whereas the same reaction at 200 MeV/nucleon yields the saturated flow as early as 40 fm/c.

In Fig. 2, we plot $\langle p_x/A\rangle$ as a function of $y_{\rm c.m.}/y_{\rm beam}$. We show each plot at a fixed energy using five different nucleon-nucleon cross sections. The (a), (b), (c), and (d) parts of the figure are at incident energy of 60, 70, 100, and 120 MeV/nucleon, respectively. Note that $\langle p_x^{\rm dir}\rangle$ vanishes at 60, 70, 100, and 120 MeV/nucleon, respectively, for the reactions with $\sigma=55$, 40 mb, Cug, and 20 mb (see Fig. 1). The slope of $\langle p_x/A\rangle$ with $\sigma=55$ mb is almost zero at 60 MeV/nucleon whereas all other cross sections yield a negative flow. In the same way, the slope of $\langle p_x/A\rangle$ vanishes at 70, 100, and 120 MeV/nucleon, respectively, for simulations with $\sigma=40$ mb, Cug/GMC, and 20 mb. One also notices that the maximum flow is seen with $\sigma=55$ mb. This is followed by $\sigma=40$ mb and Cug/GMC. Comparing Figs. 1 and 2, it is clear that $\langle p_x^{\rm dir}\rangle$ and the slope of $\langle p_x/A\rangle$ vanish at same incident energies. The $\langle p_x^{\rm dir}\rangle$ is negative at incident energies where the $\langle p_x/A\rangle$ plot yields a negative slope.

The above analysis of transverse momentum is done for nucleons only. We here neglect the formation of fragments. It is relevant that the balance energy $E_{\rm bal}$ is nearly independent of the nature of particles (i.e., it is about the same for nucleons and fragments). In Fig. 3, we look for the effect of angular distribution of the nucleon-nucleon cross section on $\langle p_x/A\rangle$ and the rapidity distribution. We here compare the results obtained with standard Cugnon cross section and isotropic Cugnon cross section. This gives us the possibility to examine the role of angular distribution in nucleonic flow

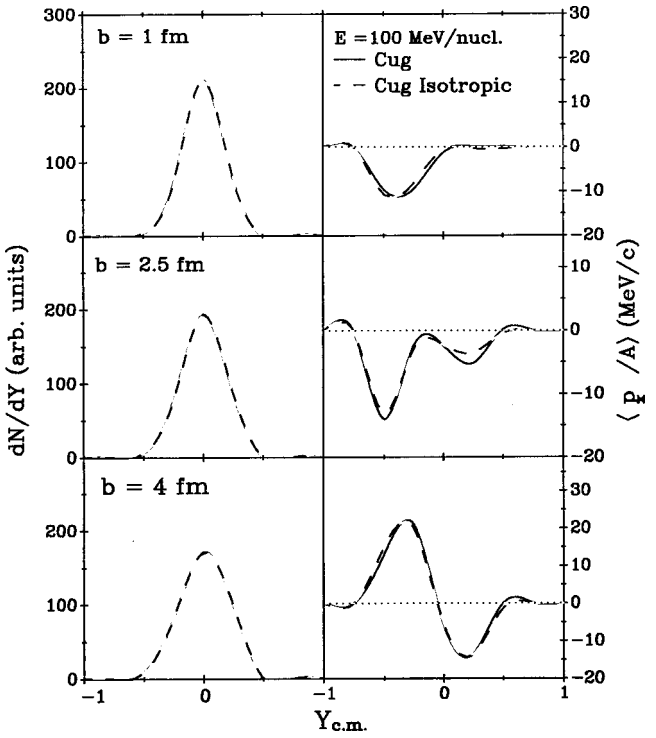

FIG. 3. $\langle p_x/A\rangle$ (right part) and rapidity distribution (dN/dY) (left part) as a function of $Y_{\text{c.m.}}$. Here we compare the results obtained with standard Cugnon and isotropic Cugnon cross sections. The results of the standard Cugnon cross section and the isotropic Cugnon cross section are represented by the solid and long dashed lines.

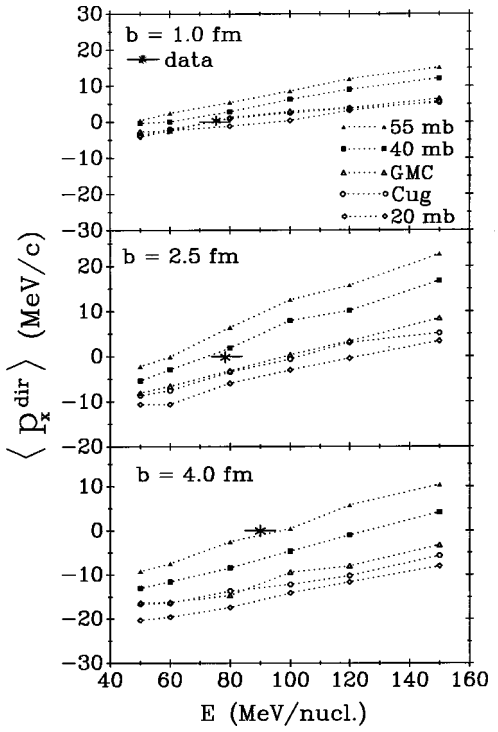

FIG. 4. The average $\langle p_x^{\text{dir}}\rangle$ as a function of incident energy. The results obtained with σ=Cug, G matrix, 55, 40, and 20 mb are shown, respectively, by circles, triangles, filled triangles, filled squares, and diamonds. The experimental data is indicated by an asterisk. The upper, middle, and lower parts of the figure are at impact parameter $b=1$, 2.5, and 4 fm, respectively.

and rapidity distribution. Note that while performing the simulation with these two cross sections, we have the same energy dependence of the cross section but a different angular dependence. The different angular dependence does not influence the nucleonic flow and their associated rapidity distribution.

In Fig. 4, we show the nucleonic flow (i.e., the transverse nucleonic flow $\langle p_x^{\text{dir}}\rangle$) as a function of incident energy E. Here we perform the simulations with a stiff equation of state. The results shown with open circles, triangles, filled triangles, filled squares, and open diamonds show the simulations with nucleonic cross sections taken from Cugnon, G matrix, a constant $\sigma=55$, 40, and 20 mb, respectively. We also show the experimental data of He *et al.* [1]. We see several points: (i) At $b=1$ fm, the standard energy-dependent cross section or in-medium G-matrix cross section explains the experimental E_{bal} nicely. The energy-dependent–G-matrix cross section starts deviating from the experimental data as we shift towards larger impact parameters. Note that the experimental E_{bal} is 75 ± 5, 79 ± 5, and 90 ± 5 MeV/c, respectively, at $b=1$, 2.5, and 4 fm, whereas the simulations with Cugnon (G-matrix) cross section predict E_{bal} at 72 MeV/c (74 MeV/c), 102 MeV/c (98 MeV/c), and 230 MeV/c (180 MeV/c), respectively, at $b=1$, 2.5, and 4 fm. As the observed balance energy at $b=4-5$ fm is an estimation, we simulate the collisions at $b=4$ fm (rather than at 4.5 fm). We see that the balance energy obtained with in-medium cross section does not differ much compared to the energy-dependent cross section. Therefore, the effect of the in-medium cross section is rather smaller as far as the vanishing of flow is concerned. E_{bal} obtained with $\sigma=55$ mb overestimates the experimental E_{bal} at $b=1$ fm, whereas it explains E_{bal} at $b=4$ fm nicely. E_{bal} at 2.5 fm can be explained nicely with a constant cross section of 40 mb. In Fig. 5, we plot the E_{bal} as a function of impact parameter. We see that a larger cross section ($\sigma=55$ mb), though it explains E_{bal} at $b=4$ fm nicely, reaches E_{bal} quite early at other impact parameters. The Cugnon parametrization explains the experimental E_{bal} at $b=1$ fm, but its slope (with an increase in the impact parameter) increases more steeply compared to other cross sections

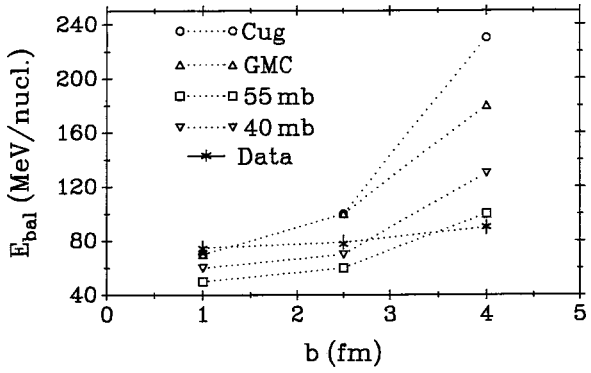

FIG. 5. The balance energy (where flow disappears) as a function of impact parameter. The balance energy obtained with the cross section due to Cugnon, G matrix, $\sigma=55$, and 40 mb are indicated by open circles, triangles, squares, and diamonds, respectively. The experimental data is shown by asterisks.

or experimental data. The in-medium cross section (GMC) does not alter the results at smaller impact parameters, it affects the balance energy at larger impact parameters. At $b=4$ fm, it reaches the zero flow quite early compared to the energy-dependent cross section. Therefore, it shows that the in-medium effects can be quite important at larger impact parameters. The failure of the standard cross section to reproduce the balance energy at larger impact parameters has also been reported in several other references [1,6,8,12]. In Ref. [8], the QMD simulations (for the Ca-Ca system) explain the $E_{\rm bal}$ at smaller impact parameters whereas it overestimates the results at larger impact parameters. Similar results are also reported for the collision of ^{64}Zn+^{27}Al [1]. This failure of the standard cross section to reproduce the experimental balance energy at large impact parameters could be resolved if one takes the momentum dependence of nuclear force into account [12]. In our case, we have an additional repulsion due to the large nucleon-nucleon cross section. Both the momentum-dependent interaction and large cross section leads to the same effect, i.e., both produce more repulsion. In the case of multifragmentation, both are found to give more fragments [17,18]. From the above findings, it is clear that there is no unique cross section which can explain the experimentally observed balance energy as a function of the impact parameter. One needs extra repulsion to explain the experimental data at larger cross sections. Similar conclusions and trends can be found in Ref. [1] where the BUU model was used to simulate the ^{64}Zn+^{27}Al reaction. There, one needs a cross section of about 45 mb to explain the data at $b=4.5$ fm. We need a larger cross section ($=55$ mb) compared to Ref. [1]. One should keep in mind that the transverse flow is a very sensitive quantity and different implementations and procedures used in the model can have appreciable effects [21]. Using the BUU model, different results of the disappearance of flow for the same reactions are also reported in Refs. [11] and [5]. One of the apparent differences is the initial boost of the nuclei and also the additional symmetry potential. Apart from different theoretical results, a comparison of the experimental results of Refs. [12] and [1] also leads to different conclusions. While going from scaled impact parameter $b/b_{\rm max}=0.28$ to 0.56 in Ref. [12], there is an increase in the balance energy by about 27 MeV, whereas for a similar increase in the impact parameter, He *et al.* [1] reports an increase of about 11 MeV. Therefore, a detailed analysis of the disappearance of flow is needed for a clearer picture.

Summarizing, we have simulated ^{64}Zn+^{27}Al at several impact parameters and over a wide range of incident energies. We have studied the balance energy (where nuclear flow vanishes). The nuclear flow studied within the QMD model gives a well-known behavior, i.e., the nuclear flow is negative at low incident energies and decreases with the increase in the bombarding energy and vanishes at same bombarding energy. With further increase in the bombarding energy, the nucleonic flow increases. The balance energy is quite sensitive towards different forms of nucleon-nucleon cross sections. We also notice that the standard energy-dependent (and in-medium) cross sections result in similar balance energies and explain the experimental data at semicentral collisions, whereas a larger value of the nucleon-nucleon cross section is needed at peripheral collisions to explain the data.

ACKNOWLEDGMENTS

This work was supported in part by Council of Scientific and Industrial Research Grant No. 03(0823)/97/EMR-II-.

[1] Z. Y. He *et al.*, Nucl. Phys. **A598**, 248 (1996).
[2] G. F. Bertsch, W. G. Lynch, and M. B. Tsang, Phys. Lett. B **189**, 384 (1987).
[3] D. Krofcheck *et al.*, Phys. Rev. Lett. **63**, 2028 (1989); D. Krofcheck *et al.*, Phys. Rev. C **46**, 1416 (1992).
[4] D. Klakow *et al.*, Phys. Rev. C **48**, 1982 (1993).
[5] H. M. Xu, Phys. Rev. C **46**, R389 (1992).
[6] J. P. Sullivan *et al.*, Phys. Lett. B **249**, 8 (1990).
[7] S. Soff, S. A. Bass, C. Hartnack, H. Stöcker, and W. Greiner, Phys. Rev. C **51**, 3320 (1995).
[8] R. Pak *et al.*, Phys. Rev. C **53**, R1469 (1996).
[9] J. C. Angelique *et al.*, Nucl. Phys. **A614**, 261 (1997).
[10] E. Lehmann, A. Faessler, J. Zipprich, R. K. Puri, and S. W. Huang, Z. Phys. A **355**, 55 (1996).
[11] B. A. Li, Phys. Rev. C **48**, 2415 (1993).
[12] R. Pak *et al.*, Phys. Rev. C **54**, 2457 (1996).
[13] A. Buta *et al.*, Nucl. Phys. **A584**, 397 (1995).
[14] G. D. Westfall *et al.*, Phys. Rev. Lett. **71**, 1986 (1993).
[15] S. Kumar, M. K. Sharma, R. K. Puri, K. P. Singh, and I. M. Govil, *Nuclear Physics Symposium*, Bangolore, 1997 (unpublished).
[16] J. Aichelin, Phys. Rep. **202**, 233 (1991).
[17] S. Kumar, R. K. Puri, and J. Aichelin, Phys. Rev. C **58**, 1618 (1998).
[18] W. F. J. Muller *et al.*, *Proceedings of the International Workshop on Gross-Properties of Nuclei and Nuclear Excitation*, Hirchegg, Austria, 1992 (unpublished), p. 50.
[19] For the Cugnon parametrization, we use the implementation of Aichelin and co-workers.
[20] A. Bohnet, N. Ohtsuka, J. Aichelin, R. Linder, and A. Faessler, Nucl. Phys. **A494**, 349 (1989); R. K. Puri, N. Ohtsuka, E. Lehmann, A. Faessler, M. A. Matin, D. T. Khoa, G. Batko, and S. W. Huang, *ibid.* **A575**, 733 (1994).
[21] C. Hartnack, R. K. Puri, J. Aichelin, J. Konopka, S. A. Bass, H. Stoecker, and W. Greiner, Eur. Phys. J. A **1**, 151 (1998).